ACI MATERIALS JOURNAL TECHNICAL PAPER

Title No. 119-M21

Mechanical Properties of Alkali-Silica Reaction-Affected Concrete

by Anca C. Ferche and Frank J. Vecchio

Experiments focusing on the mechanical behavior of plain alkali-silica reaction (ASR)-affected concrete were undertaken. Cube specimens, 150 x 150 x 150 mm (6 x 6 x 6 in.) in dimensions, standard 100 mm (4 in.) Φ concrete cylinders, and 75 x 75 x 285 mm (3 x 3 x 11.2 in.) concrete prisms were cast with nonreactive aggregate, reactive fine aggregate (Jobe-Newman), or reactive coarse aggregate (Spratt). To accelerate the rate of the reaction, the specimens were conditioned under elevated humidity and temperature. The investigation was designed to allow the development of differential expansion along orthogonal directions in cube specimens as a result of different levels of externally applied stress. Cylindrical cores were extracted along each differently loaded direction from cubes experiencing similar stress conditions and were tested in compression and tension. In addition, tests were performed on specimens that were conditioned in a stress-free state.

It was found that ASR-induced deterioration affected differently the compressive strength, modulus of elasticity, and tensile strength of the concrete cured in stress-free conditions. Tests on cores extracted from the restrained cubes revealed that the mechanical properties of ASR-affected concrete were direction-dependent as anisotropic degradation of the mechanical properties developed.

Keywords: alkali-silica reaction (ASR); direction-dependent mechanical properties; mechanical properties; stiffness deterioration; strength reduction; tensile strength.

INTRODUCTION

Deleterious alkali-silica reaction (ASR) develops when a concrete mixture contains aggregate susceptible to alkali attack. The chemical reactions between the alkali hydroxides from the cement paste and certain siliceous minerals produce a hygroscopic gel that absorbs water and swells if moisture is available. The pressure buildup resulting from the gel expansion causes cracking of the concrete matrix, which in turn leads to deterioration of the mechanical properties of ASR-susceptible concrete. In addition, ASR-induced cracking is most likely to bring serious consequences regarding the long-term durability of reactive structures, including acceleration of mechanisms such as chemical attack and reinforcement corrosion.

Since it was first identified by Stanton,[1,2] a variety of structures have been diagnosed as suffering from ASR, from dams and nuclear power plant structures to bridges and parking structures. The Sixth Street Viaduct in Los Angeles, CA,[3] and several highway bridges in the Netherlands,[4] Denmark,[5] and Canada,[6] for example, have had to be demolished due to extensive ASR-induced damage (Fig. 1).

Knowledge of concrete's mechanical behavior is essential for reliable structural assessment; as such, various

Fig. 1—ASR-affected column and foundation block of Robert-Bourassa/Charest Bridge, Canada, demolished in 2010 (taken from Sanchez et al.[6]).

laboratory studies have been undertaken to characterize the response of ASR-affected concrete. The majority of the tests were performed on concrete specimens conditioned in an unrestrained state that developed randomly oriented cracks resulting in a map-cracking pattern. The primary goal of these experiments was to investigate factors that influence ASR expansion and its effect on concrete mechanical properties. The influencing factors examined included particle size,[7] casting direction,[8] degree of reactivity of the aggregate,[9] alkali content,[10] environmental conditions,[11,12] and air entrainment.[13] In addition, substantial research effort has been directed toward studying the effect of sustained long-term restraint on the development of ASR.[14-19] By contrast, the deterioration of the mechanical properties of

ACI Materials Journal, V. 119, No. 1, January 2022.

MS No. M-2021-019.R1, doi: 10.14359/51734198, received June 2, 2021, and reviewed under Institute publication policies. Pertinent discussion including author's closure, if any, will be published ten months from this journal's date if the discussion is received within four months of the paper's print publication.

ASR-affected concrete subjected to long-term loading has been less investigated.

Studies[20-22] have found that the mechanical properties of ASR-affected concrete are highly influenced by the level of expansion and by the orientation of the crack planes, both of which are linked to the sustained long-term stress conditions. The test program presented herein was designed to investigate this ASR-induced anisotropy in the mechanical properties through compressive and splitting tensile tests performed on cores extracted from cubes that were subjected to different long-term compressive stresses along orthogonal directions.

The nature of this anisotropy lies within the characteristics of the ASR-induced damage itself. The level of expansion and the direction of the ASR-induced crack planes are directly influenced by the three-dimensional stress state. In most structures, concrete experiences different levels of sustained stress along different directions. Thus, the ASR-induced damage exhibits variations that are direction-dependent. In addition to the stresses induced by service loading, an ASR-affected concrete element subjected to external or internal restraints develops compressive stresses within the concrete component as a result of the ASR expansion. The magnitude of the ASR-induced compressive stresses is influenced by the level of restraint (for example, reinforcement ratio, service load-induced stresses, nature of boundary conditions) and by the reactivity of the concrete.

RESEARCH SIGNIFICANCE

Data available in the literature suggest a strong dependence of the mechanical properties of ASR-affected concrete on the severity of expansion and on the predominant crack plane direction, both linked to the long-term stress conditions, leading to various degrees of anisotropy. The test program presented in this paper was developed to quantify this anisotropy. The results obtained add data to a currently limited database and constitute a foundation for the formulation of constitutive models suited for advanced modeling and structural assessment.

TEST PROGRAM

Specimen description

The test program involved the construction of 150 x 150 x 150 mm (6 x 6 x 6 in.) concrete cubes, cast with nonreactive, reactive fine (Jobe-Newman), or reactive coarse (Spratt) aggregate. The cubes were subjected to different three-dimensional stress states during the curing period, applied through external loading frames.

At the end of the conditioning period, the loading frames were removed and 75 mm (3 in.) Φ cores were drilled along each differently loaded orthogonal direction. Uniaxial compression and splitting tensile tests were performed on the cores. The mechanical properties of interest were compressive strength, modulus of elasticity, strain at peak stress, Poisson's ratio, and splitting tensile strength.

The stress conditions applied to the cube specimens and the testing method are presented in Table 1, along with the type of aggregate used in the concrete mixture for each cast. Each set of cubes was cast along with three 75 x 75 x 285 mm (3 x 3 x 11.2 in.) plain concrete prisms for expansion measurements and six standard 100 mm (4 in.) Φ concrete cylinders for compressive strength evaluation.

The concrete mixture design (Table 2) was based on the proportions suggested in ASTM C1293[23] with slight adjustments. Trial batches produced concrete with a reduced workability and an average 28-day compressive strength of 52 MPa (7500 psi). For the purpose of this study, the grading of the coarse aggregate and the water-cement ratio (*w*/*c*) were modified to increase the workability of the fresh concrete. The maximum aggregate size was limited to 9.5 mm (0.37 in.), compared to 19.0 mm (0.75 in.) in the standard mixture design, and the *w*/*c* was increased to 0.50.

The control mixture contained nonreactive fine and coarse aggregate, obtained from a local source. Two reactive mixtures were investigated: one containing reactive coarse aggregate and nonreactive fine aggregate and the other one containing reactive fine aggregate and nonreactive coarse aggregate. The reactive coarse aggregate was Spratt aggregate from Stittsville, ON, Canada, supplied by the Ministry of Transportation of Ontario. Spratt aggregate is slightly siliceous, with 9% SiO_2, and meets the physical requirements for concrete aggregate.[24] The reactive fine aggregate was Jobe-Newman sand from El Paso, TX, provided by The University of Texas at Austin. The sand was found to be highly reactive for both laboratory conditions and field exposure.[25]

General-use cement with a total alkali content of 0.96% Na_2O equivalent by mass of cement was used for all casts. The chemical composition of the cement is shown in Table 3. The alkali content was supplemented for the reactive mixtures by adding sodium hydroxide (NaOH) to reach a total of 1.25% Na_2O equivalent by mass of cement. The nonreactive cast did not have the alkali content boosted.

The specimens were moist-cured for a total of 72 hours, after which they were stored at ambient temperature, 21°C (70°F), until the accelerated conditioning protocol started.

Long-term load application—Approximately 30 days before the conditioning started, the cube specimens were loaded to the stress states described in Table 1. The loading was applied through external steel loading frames. Shown in Fig. 2 is a typical biaxially loaded cube specimen. Zinc-plated low-strength steel threaded rods were tensioned up to the yield stress to ensure a constant applied stress throughout the conditioning period. This procedure was similar to the one used by Gautam and Panesar[26] to apply long-term stresses on concrete cubes undergoing ASR expansion, which consisted of post-tensioning debonded rods up to yield against bearing plates placed symmetrically on the surfaces of the cube.

Two different diameters were selected for the threaded rods, 8 and 11 mm (5/16 and 7/16 in.), with a specified tensile strength of 345 MPa (50,000 psi). The mechanical properties of the rods were determined from uniaxial tension tests. The rods were delivered in lengths of 6.1 m (20 ft); however, it was not certain they were all from the same batch. Therefore, because the stress-strain response of the rods had a significant influence on the applied loading on the cubes, a 250 mm (9.8 in.) coupon was tested from each length.

Table 1—Cube specimen test matrix

Cubes set	No. of cubes	σ_x, MPa	σ_y, MPa	σ_z, MPa	Test method	Cast date	Reactive aggregate
N1	4	0.00	0.00	0.00	Compression	June 12, 2017	None
	4	0.00	0.00	0.00	Tensile splitting		
R1	3	4.22	2.57	0.00	Compression	June 14, 2017	Spratt
	1	0.00	0.00	0.00			
	3	4.22	2.57	0.00	Tensile splitting		
	1	0.00	0.00	0.00			
R2	3	4.22	2.57	0.00	Compression	June 16, 2017	Jobe-Newman
	1	0.00	0.00	0.00			
	3	4.22	2.57	0.00	Tensile splitting		
	1	0.00	0.00	0.00			
R3	2	4.22	0.00	0.00	Compression	June 19, 2017	Spratt
	1	0.00	0.00	0.00			
	2	4.22	0.00	0.00	Tensile splitting		
	1	0.00	0.00	0.00			
R4	2	4.22	0.00	0.00	Compression	June 21, 2017	Jobe-Newman
	1	0.00	0.00	0.00			
	2	4.22	0.00	0.00	Tensile splitting		
	1	0.00	0.00	0.00			
R5	3	8.44	4.22	0.00	Compression	June 23, 2017	Spratt
	1	0.00	0.00	0.00			
	3	8.44	4.22	0.00	Tensile splitting		
	1	0.00	0.00	0.00			

Note: 1 MPa = 145 psi.

Table 2—Concrete mixture design

	ASTM C1293	Current mixture
Cement, kg/m^3	420	410
Water, kg/m^3	185	205
Fine aggregate, kg/m^3	721	730
Coarse aggregate, kg/m^3	1113	1000
w/c	0.42	0.50
Unit weight, kg/m^3	2440	2345
28-day strength, MPa	52	42

Note: 1 kg/m^3 = 0.062 lb/ft^3; 1 MPa = 145 psi.

Table 3—Chemical composition of general-use cement

	%
L.O.I.	1.93
SiO_2	19.05
Al_2O_3	5.12
Fe_2O_3	2.46
CaO	62.52
MgO	2.47
SO_3	4.05
Free lime	1.375
Na_2Oeq	0.96

Note: L.O.I. is loss on ignition.

The yield stress and the corresponding yield strain were determined using the 0.2% offset method as the stress-strain response of the rods did not present a clearly defined yielding plateau. As such, a variation of up to 9% in the sustained stress level potentially developed. The stress-strain relationships for the threaded rods and their properties are given in Appendix A.* The 8 mm (5/16 in.) rods had an average yield stress of 422 MPa (61,200 psi) and a corresponding yield strain of 4.32×10^{-3}, while the 11 mm (7/16 in.) rods had an average yield stress of 444 MPa (64,400 psi) and a yield strain of 4.09×10^{-3}.

To ensure that the rods were tensioned to the same level of stress, a load-torque correlation procedure was performed. A 500 kN (112 kip) load cell was placed between two 150 mm (6 in.) square steel plates (Fig. 3). The loading frame was then set up to encompass them as it would the concrete cubes. The total height of the stiff steel plates and load cell was similar to the height of the cube. A torque wrench was used to tension the rods progressively in small increments.

*The Appendix is available at **www.concrete.org/publications** in PDF format, appended to the online version of the published paper. It is also available in hard copy from ACI headquarters for a fee equal to the cost of reproduction plus handling at the time of the request.

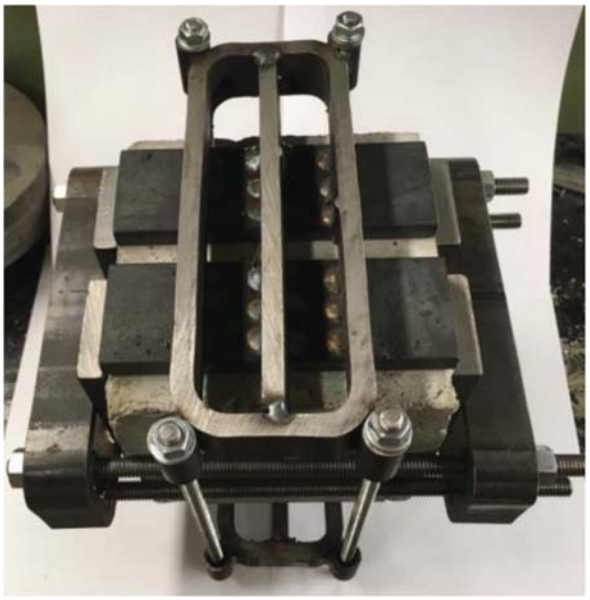

Fig. 2—Biaxially loaded cube.

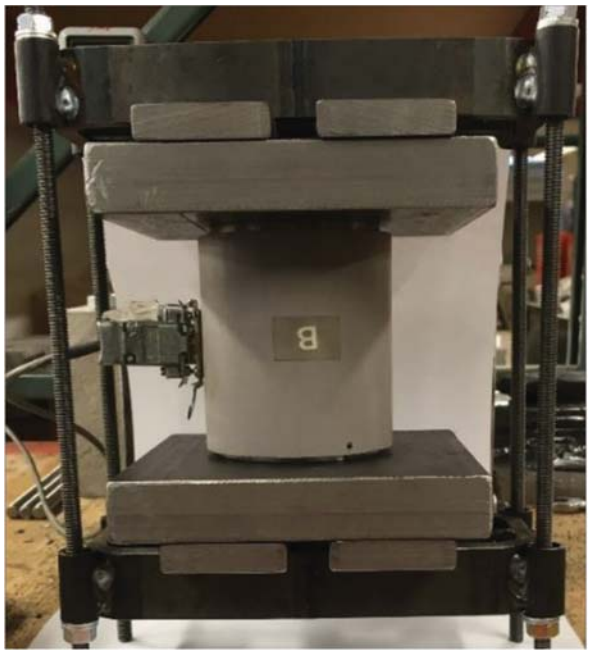

Fig. 3—Load-torque correlation setup.

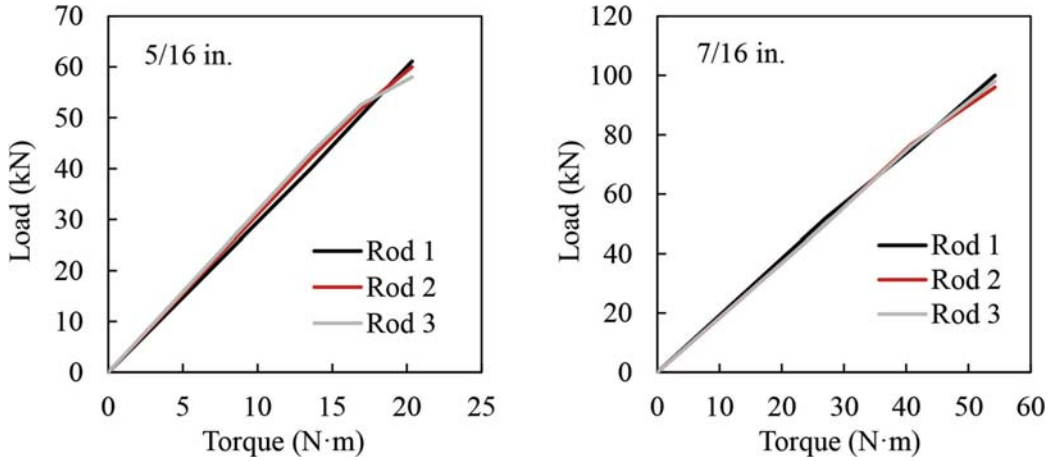

Fig. 4—Total load-torque relationships.

Figure 4 shows the load-torque relationships. Three tests were performed for each different rod diameter to give an indication of the procedure's consistency. Virtually identical linear relationships were obtained. In addition, to monitor the strain, the elongations of the rods were measured with a digital gauge set on a specially designed frame.

Accelerated conditioning and expansion measurement

All specimens were placed inside an environmentally controlled chamber to accelerate the reaction. At the time the accelerated conditioning protocol started, the ages of the specimens were 319 days for Cast N1, 317 days for Cast R1, 315 days for Cast R2, 312 days for Cast R3, 310 days for Cast R4, and 308 days for Cast 5. The specimens were placed on steel wire mesh racks, as shown in Fig. 5, with sufficient space between them to allow uniform moisture ingress. The steel plates of the restrained cube specimens were 51 mm (2 in.) wide, covering 67% of the surfaces they were bearing on. This, however, was not considered to have significantly influenced the moisture content within the cube specimens. The sides of the cubes corresponding to the stress-free direction were not covered, thus permitting unrestricted moisture penetration. As the dimensions of the cube specimens were relatively small, the moisture penetrating from the unrestrained sides was expected to produce a uniform moisture distribution profile, given the long-term conditioning period.

The specimens were maintained at a constant temperature of 50 ± 0.5°C (122 ± 0.9°F) and 97 ± 3% relative humidity. The temperature and relative humidity were chosen based on two objectives: to increase the inherently slow rate of ASR expansion; and to minimize the effects overly accelerated conditioning may have upon the response of the concrete.

The most widely used temperature for laboratory studies on ASR is 38°C (100°F). The tests carried out by Locher and Sprung[27] found a pessimum value of 38°C (100°F) for which the ASR expansion is the largest. Additionally, CSA A23.2-14[28] and ASTM C1293[23] suggest a temperature of 38°C (100°F) for assessing the reactivity of aggregates. At this temperature, the ASR expansion is usually exhausted after

Fig. 5—Specimens inside environmental chamber.

1 to 2 years. Gautam and Panesar[11] investigated the effect of elevated conditioning temperature on the ASR expansion, and they found that increasing the temperature from 38 to 50°C (100 to 122°F) increased the rate of the reaction by a factor of 3.22. The relative humidity for both temperatures was greater than 95%. The trend of the expansion, the ultimate expansion, and the mechanical properties investigated were not influenced by the increased temperature. The Damage Rating Index method showed a slight increase in the extent of damage and microstructural cracking for the concrete subjected to 50°C (122°F), suggesting that the response of ASR-affected concrete subjected to accelerated conditioning is somewhat different than concrete in field structures. Nevertheless, accelerating the rate of the reaction is, in most cases, necessary when studying ASR.

Periodic expansion measurements were taken following the procedure outlined by ASTM C1293 to monitor the unrestrained longitudinal strains of the prisms, stored in the same environmental conditions as the cubes and cylinders for correlation purposes. Strain measurements were also performed on the unrestrained cubes. Stainless steel targets were glued with structural epoxy on opposing faces of the cubes and a rigid steel frame was used to perform the measurements.

The shrinkage strains measured on the expansion prisms prior to the beginning of the accelerated conditioning averaged to a value of 0.72×10^{-3} for all casts. Given in Appendix B are the strain measurements performed on prisms before the conditioning period.

The evolution of the expansion during the conditioning period is shown in Fig. 6(a) for the prisms and in 6(b) for the cubes. The strains reported for the prisms represent the average of three measurements taken on three different prisms for each cast. For each cube specimen, four strain measurements were taken.

The average strain measured on prisms of the nonreactive mixture at the end of the conditioning period, after 259 days of curing, was 0.34×10^{-3}, below the 0.40×10^{-3} threshold imposed by ASTM C1293 to identify reactive mixtures. The expansion of the nonreactive mixture was relatively constant after 68 days in the environmental chamber and was primarily attributed to swelling due to absorption of water by the cement paste. Another potential mechanism contributing to the expansion of the nonreactive mixture could have been the presence of a small amount of reactive minerals within the aggregates classified as nonreactive.

Expansion strains measured on prisms corresponding to the reactive mixtures all exceeded the strain threshold for reactivity suggested by ASTM C1293 (Fig. 6(a)). The Spratt mixtures developed lower ASR-induced strains compared to data reported by researchers[11,29] using the same type of reactive aggregate, mainly due to the higher *w/c* used in the current mixture potentially having led to increased porosity of the hardened concrete. With increased porosity, a larger amount of ASR gel was accommodated within the concrete matrix before expansion developed. The Jobe-Newman mixtures were substantially more reactive compared to the Spratt ones. The reactive mixtures all exhibited a change in the rate of expansion after 133 days in the conditioning room. This was caused by the installation of sprinklers within the environmental chamber that were meant to enhance moisture ingress within the concrete specimens.

The strains measured from cubes (Fig. 6(b)) were higher for all mixtures compared to the strains measured from prisms, while the rate of the expansion was similar for both prisms and cube specimens. Given that the ASR-induced expansion is influenced by the size of the specimens, these results are consistent with data reported in the literature.

Test setups and instrumentation

At the end of the conditioning period, the cubes were removed from the environmental chamber and the loading frames were detached. Cores were drilled along each orthogonal stress direction with a 75 mm (3 in.) Φ diamond drill bit. Uniaxial compression tests and splitting tensile tests were performed 24 hours after extraction to determine the mechanical properties along the directions of interest.

Uniaxial compression test—Uniaxial compression tests were performed to obtain the compression stress-strain response, the compressive strength, the modulus of elasticity, and the Poisson's ratio. Before testing, the ends of the specimens were ground smooth using a cylinder grinding machine to avoid uneven loading caused by surface imperfections and to ensure that the ends were parallel to each other. A stiff frame machine with a load capacity of 4500 kN (1012 kip) was used to perform the compression tests. The test specimens were instrumented with two ±2.5 mm (±0.098 in.) stroke linear variable differential transformers (LVDTs), set up diametrically opposite over a gauge length of 115 mm (4.5 in.) for the cores and 152 mm (6.0 in.) for the cylinders. The tests were displacement-controlled at a rate of 0.0033 mm/s (1.3×10^{-4} in./s) for the cores and 0.0067 mm/s (2.6×10^{-4} in./s) for the cylinders. The Poisson's ratio was measured using an axial extensometer. Shown in Fig. 7(a) is a typical test setup for the drilled core specimens tested.

The procedures outlined in ASTM C39[30] were followed to determine the compressive strength of the specimens. Recommendations from ASTM C469[31] were used for determining the modulus of elasticity and Poisson's ratio.

Splitting tensile test—The splitting tensile tests were performed in accordance with ASTM C496[32] on cores

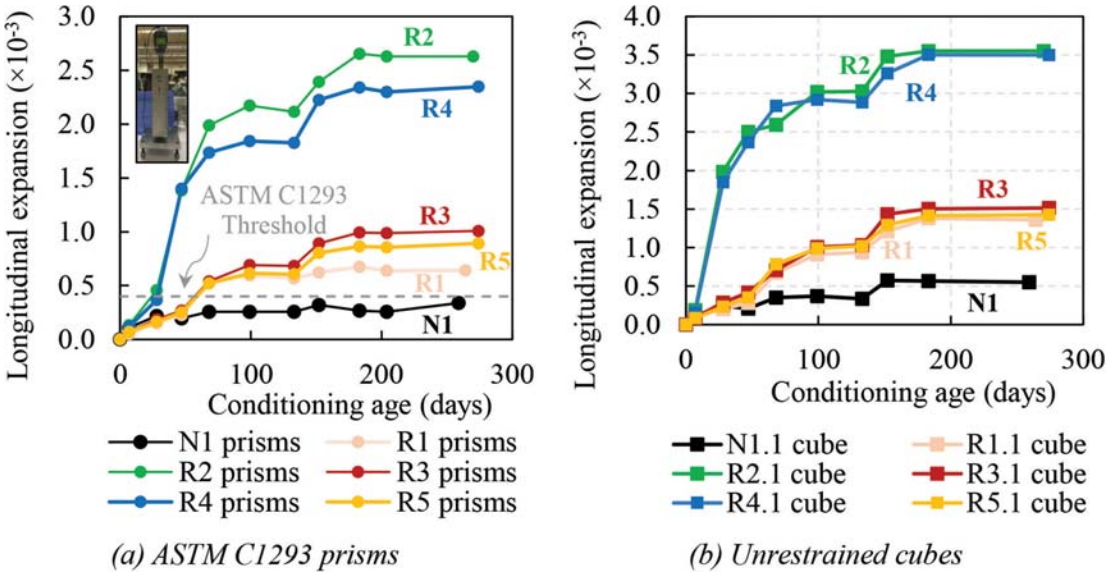

Fig. 6—ASR-induced expansion.

drilled along each orthogonal stress direction, as per Table 1. Shown in Fig. 7(b) is the splitting tensile test setup. Thin plywood bearing strips were placed along the length of the cores to distribute the load. The 4500 kN (1012 kip) stiff frame machine was used to perform the tests under force-controlled conditions, at a loading rate of 0.7 MPa/min (0.102 ksi/min).

TEST RESULTS

This section presents the test results obtained from the standard cylinder and core specimens tested. More comprehensive test results and analyses are presented elsewhere.[33]

Mechanical properties evolution of unrestrained 4 in. Φ cylinder specimens

Three standard 100 mm (4 in.) Φ × 200 mm (8 in.) cylinders were tested in uniaxial compression at 28 days and post-conditioning for each of the six batches. Although the concrete mixture design was similar, inherent batch-to-batch variability in the stress-strain response was measured at 28 days. The principal sources of batch-to-batch variation applicable to the present work are variations in aggregate characteristics and potential changes in *w*/*c* caused by variation of fine aggregate moisture conditions. The average results for each batch at 28 days are summarized in Table 4 in terms of peak stress f_c' and modulus of elasticity E_c. The stress-strain relationships are shown in Appendix C for all tests. The batches containing reactive fine Jobe-Newman aggregate, R2 and R4, resulted in concrete mechanical properties somewhat closer to the nonreactive batch, N1, compared to the batches containing reactive coarse Spratt aggregate, R1, R3, and R5. In all specimens, the cracks propagated through the coarse aggregate, indicating that the aggregate strength had a dominant effect on the concrete strength. This type of failure is expected for concrete containing limestone coarse aggregate.[34] Consistent with this mechanism, across the batches, the average concrete properties reflect different coarse aggregate used in the mixture.

Post-conditioning, the mechanical properties measured from cylinders showed a significantly higher batch-to-batch variability compared to the one observed at 28 days, owing to the ASR-induced damage. The average results for the peak stress f_{cp} and modulus of elasticity $E_{c,PC}$, measured at the end of the conditioning period, along with the ASR-induced strain measured on prisms ε_{ASR}, are summarized in Table 4. The strength and stiffness of the reactive concrete were found to be influenced differently by ASR.

Compared to the 28-day values, the peak stress measured post-conditioning, f_p, increased for the nonreactive mixture N1 and for the reactive mixtures cast with reactive coarse Spratt aggregate R1, R3, and R5, by 33%, 28%, 32%, and 34% respectively. No significant change in peak stress was measured for the reactive mixtures cast with reactive Jobe-Newman fine aggregate, R2 and R4. The more severe expansion experienced by the R2 and R4 specimens ultimately counteracted the usually increasing strength associated with the hydration process, resulting in virtually no change in the compressive strength. A different pattern was observed for the modulus of elasticity, which increased by 16% in the case of the nonreactive mixture and decreased for all the reactive mixtures by 15 to 28% (Table 4). Given in Appendix C are the full stress-strain responses. Post-conditioning, all casts showed a somewhat steeper slope of the stress-strain descending branch compared to the corresponding 28-day behavior.

Influence of sustained long-term stresses on mechanical properties of ASR-affected concrete

This section explores the induced anisotropy in the mechanical properties of ASR-affected concrete as a result of sustained long-term stresses. A summary of the test data is presented in Table 5 as obtained from concrete cores tested in uniaxial compression and in splitting tension. The mechanical properties are summarized in terms of concrete compressive strength at test day f_{cp}, concrete modulus of elasticity $E_{c,PC}$, splitting tensile strength f_{sp}, and Poisson's ratio μ. The cores labeled 0.0, 2.6, 4.2, and 8.4 MPa were extracted from

Table 4—Average mechanical properties of standard cylinder specimens

Cast	At 28 days		Post-conditioning		
	f_c', MPa	E_c, MPa	ε_{ASR}, × 10^{-3}	f_{cp}, MPa	$E_{c,PC}$, MPa
N1	45.9	30,200	0.34*	61.1	34,900
R1	40.1	30,100	0.64	51.3	25,700
R2	42.7	31,600	2.63	46.0	23,800
R3	38.6	29,500	1.01	50.9	23,000
R4	46.6	31,200	2.35	46.0	22,600
R5	38.0	28,500	0.89	50.8	23,400

*Expansion primarily attributed to swelling due to water absorption.

Note: 1 MPa = 145 psi.

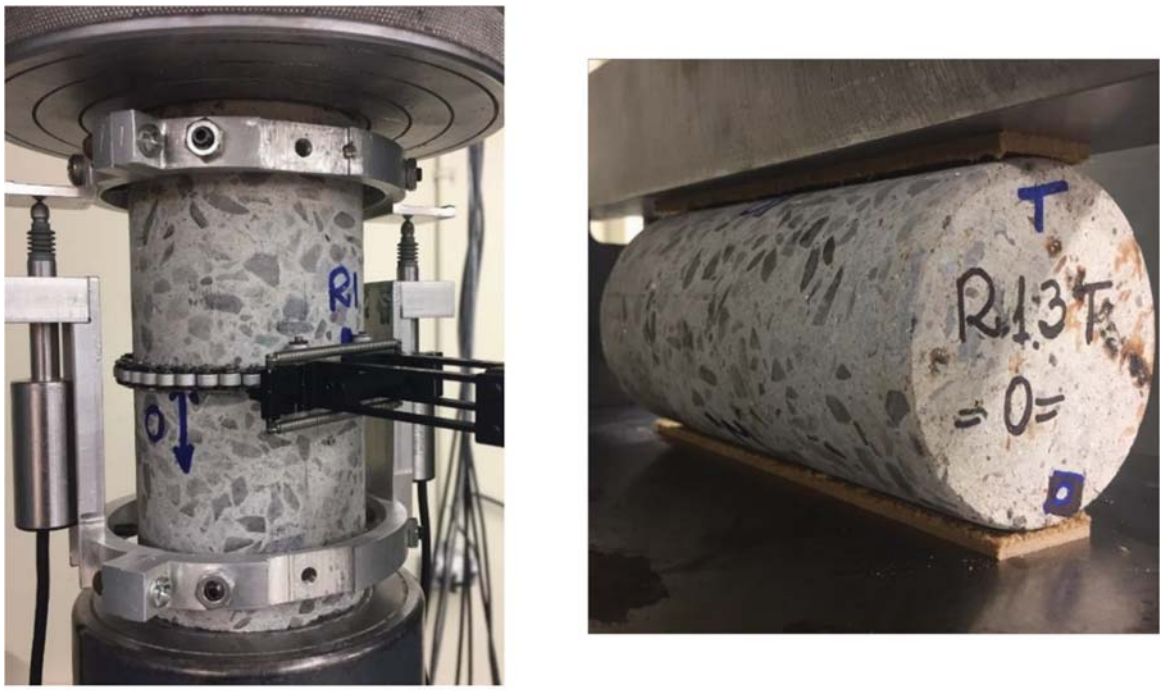

(a) Compression test setup (b) Splitting tensile test setup

Fig. 7—Typical test setups.

cubes subjected to long-term biaxial or uniaxial stresses. The coring direction was parallel to the direction of the long-term stress level indicated by the label. The cores labeled *free* were extracted from cubes that were unrestrained during the conditioning period. This designation is consistent throughout this paper. Table 5 also indicates for each cast the ASR-induced expansion, ε_{ASR}, measured on prisms. In addition, Fig. 8, 9, 10, 11, and 12 show the compressive stress-strain responses for the cores of each cast.

Apart from the long-term stress condition, one of the key influencing factors affecting the mechanical properties is the level of induced expansion. For the Spratt reactive cores, the free ASR expansion varied significantly across the casts: 0.64×10^{-3} for R1, 0.89×10^{-3} for R2, and 1.01×10^{-3} for R3. The Jobe-Newman casts showed a reduced variation in expansion, with 2.63×10^{-3} for R2 and 2.35×10^{-3} for R4.

The comparison of the response of 100 mm (4 in.) Φ cylinders tested at 28 days with that of 75 mm (3 in.) Φ cores extracted from cubes post-conditioning may result in behavior discrepancies originating from the difference in size and type of the specimens. Appendix D discusses this potential issue.

A minimum of two reference points are needed when quantifying the deterioration of concrete mechanical properties due to ASR-induced damage. These are the 28-day values and the values of the mechanical properties at test day corresponding to a similar sound concrete. This is mainly due to the time-dependent nature of the deterioration of the mechanical properties. In addition, the degradation mechanism is concurrent with processes such as continuing hydration, which influences the evolution of the mechanical properties in time.

Compressive strength—The post-conditioning compressive strength of all cores increased compared to the 28-day values. The increase in compressive strength ranged from 3% for the unrestrained R4 core to 64% for the restrained direction of the R3 core. On average, the Spratt cores showed an increase in strength comparable to that measured for the

Table 5—Post-conditioning mechanical properties of 3 in. Φ cores

Core	f_{cp}, MPa	$E_{c,PC}$, MPa	f_{sp}, MPa	μ	$E_{c,CSA}$, MPa	$E_{c,ACI}$, MPa	$E_{c,PC}/E_{c,CSA}$	$E_{c,PC}/E_{c,ACI}$
N1, Nonreactive: $\varepsilon^* = 0.034 \times 10^{-3}$								
1	64.3	33,800	5.19	0.16	33,400	37,700	1.01	0.90
2	63.1	33,000	5.43	0.17	33,100	37,300	1.00	0.88
3	64.2	34,200	5.20	0.16	33,400	37,700	1.02	0.91
Average	63.9	33,700	5.27	0.17	33,300	37,600	1.01	0.90
R1, $\varepsilon_{ASR} = 0.64 \times 10^{-3}$								
0.0 MPa	58.4	22,100	4.21	0.16	32,100	35,900	0.69	0.62
2.6 MPa	58.3	27,400	4.34	0.14	32,100	35,900	0.85	0.76
4.2 MPa	46.6	28,400	4.12	0.18	29,400	32,100	0.96	0.88
free	47.7	23,500	3.59	0.15	29,700	32,500	0.79	0.72
R2, $\varepsilon_{ASR} = 2.63 \times 10^{-3}$								
0.0 MPa	56.1	23,600	3.82	0.19	31,600	35,200	0.75	0.67
2.6 MPa	59.0	23,800	5.07	0.19	32,300	36,100	0.74	0.66
4.2 MPa	53.2	24,000	3.97	0.20	31,000	34,300	0.77	0.70
free	47.4	25,600	3.73	0.14	29,600	32,400	0.86	0.79
R3, $\varepsilon_{ASR} = 1.01 \times 10^{-3}$								
0.0 MPa	53.7	20,600	4.03	0.11	31,100	34,400	0.66	0.60
4.2 MPa	63.4	32,500	3.76	0.13	33,200	37,400	0.98	0.87
free	56.8	24,400	3.47	0.11	31,800	35,400	0.77	0.69
R4, $\varepsilon_{ASR} = 2.35 \times 10^{-3}$								
0.0 MPa	53.0	23,200	4.16	0.17	31,000	34,200	0.75	0.68
4.2 MPa	52.9	26,900	3.62	0.15	30,900	34,200	0.87	0.79
free	48.1	25,500	4.01	0.13	29,800	32,600	0.86	0.78
R5, $\varepsilon_{ASR} = 0.89 \times 10^{-3}$								
0.0 MPa	49.2	24,600	4.74	0.15	30,100	33,000	0.82	0.75
4.2 MPa	53.0	27,000	3.81	0.17	30,900	34,200	0.87	0.79
8.4 MPa	60.4	28,700	5.12	0.15	32,500	36,500	0.88	0.78
free	57.7	23,300	3.86	0.14	32,000	35,700	0.73	0.65

*Expansion primarily attributed to swelling due to water absorption.

Note: 1 MPa = 145 psi.

nonreactive specimens. These results are in agreement with data reported in the literature,[21,35] and they indicate that the ASR-induced deterioration of the Spratt concrete did not exceed the threshold to cause deterioration of the compressive strength.

The post-conditioning compressive strength of the Jobe-Newman cores was higher compared to the 28-day value; however, this increase was on average smaller than the one measured for the Spratt and the nonreactive cores. Anisotropy of the compressive strength based on long-term stress condition was measured for the Jobe-Newman specimens. The strengths of the cores extracted from the restrained cubes (0.0, 2.6, and 4.6 MPa) were higher compared to the unrestrained cubes (labeled as *free*). In this case, the long-term compressive stresses had a beneficial effect on the compressive strength compared to the unrestrained specimens.

Modulus of elasticity—The tests on the Spratt specimens generally showed that sustained compressive stresses had a beneficial effect on the evolution of the modulus of elasticity. For all three sets of cubes (R1, R3, and R5), the stiffness in the direction of the long-term compressive stresses did not change significantly compared to the 28-day value. However, the cores extracted along unrestrained directions, whether they corresponded to cubes subjected to long-term stresses (0.0 MPa) or cubes that were unrestrained (*free*), all showed a reduction in the modulus of elasticity. The sets of cores pertaining to the Jobe-Newman casts all showed a reduction in stiffness with respect to the 28-day values, regardless of the coring orientation or the long-term stress condition.

CSA A23.3-14[36] and ACI 318-19[37] equations (Eq. (1) and (2)) were used to express the modulus of elasticity as a function of the compressive strength, and the results are shown in Table 5. A comparison of the results obtained using the code equations ($E_{c,CSA}$ and $E_{c,AACI}$) and the post-conditioning measured modulus of elasticity ($E_{c,PC}$) reveals that the code

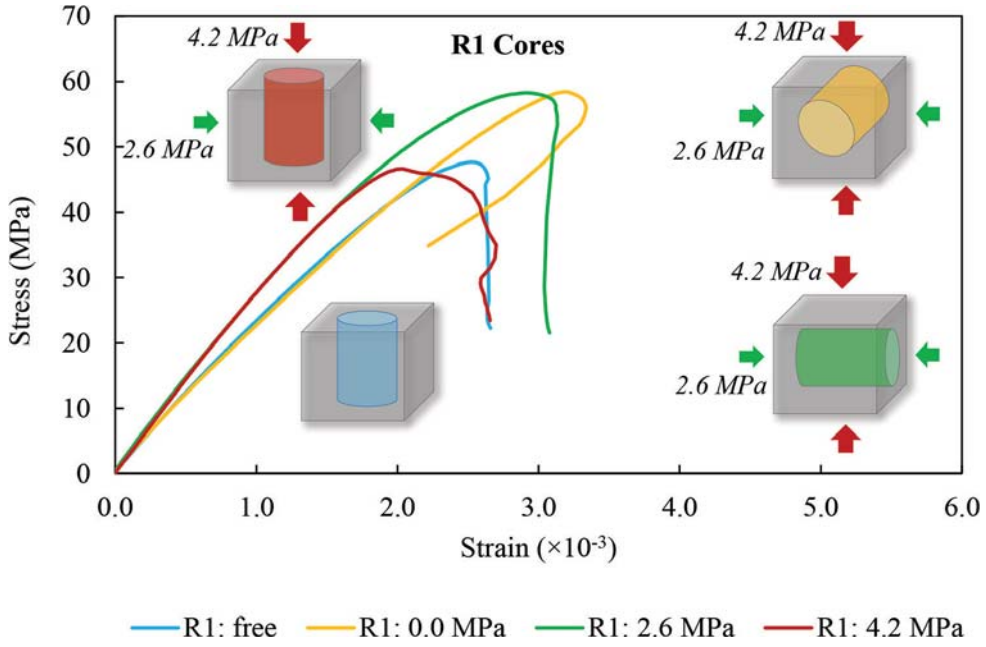

Fig. 8—Compression response R1 post-conditioning 3 in. Φ cores. (Note: 1 MPa = 145 psi.)

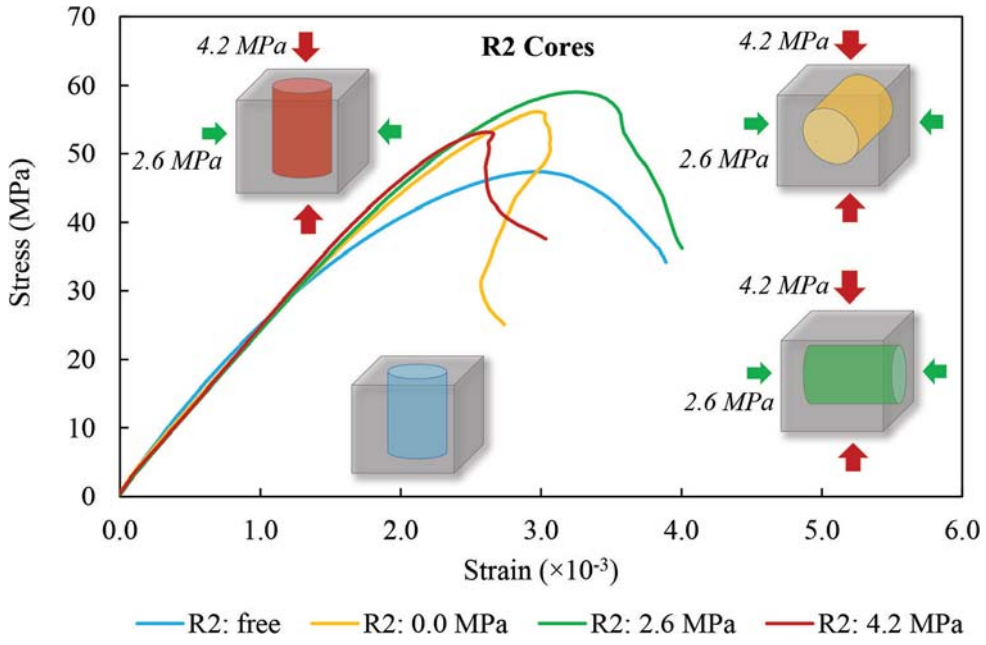

Fig. 9—Compression response R2 post-conditioning 3 in. Φ cores. (Note: 1 MPa = 145 psi.)

equations are unconservative in estimating the modulus of elasticity of ASR-affected concrete. ACI 318 was less conservative compared to CSA A23.3 for each specimen, including the nonreactive cores

$$E_{c.CSA} = \left(3300\sqrt{f_c'} + 6900\right)\left(\frac{\gamma_c}{2300}\right)^{1.5} \text{(MPa)} \quad (1)$$

$$E_{c.ACI} = 4700\sqrt{f_c'} \text{(MPa)} \quad (2)$$

where f_c' is the concrete compressive strength, measured at test day; and γ_c is the density of concrete, taken as 2300 kg/m^3 (144 lb/ft^3).

CSA A23.3 values better matched the test results in the direction of the long-term stresses for the Spratt cores. This result is consistent with the fact that for these cores, the stiffness was not reduced compared to the 28-day values. Both code predictions gave unconservative estimates for the modulus of elasticity of the Jobe-Newman cores, regardless of the stress condition or coring direction, with the ACI 318 equation being somewhat more unconservative.

Splitting tensile strength—Long-term compressive stresses had a beneficial effect on the splitting tensile strength of the Spratt specimens regardless of the coring direction (Table 5). An increase of 33% in the splitting tensile strength was measured along the third principal direction (8.4 MPa) of the R5 cubes and of 23% along the first principal direction (0.0 MPa). As such, the long-term

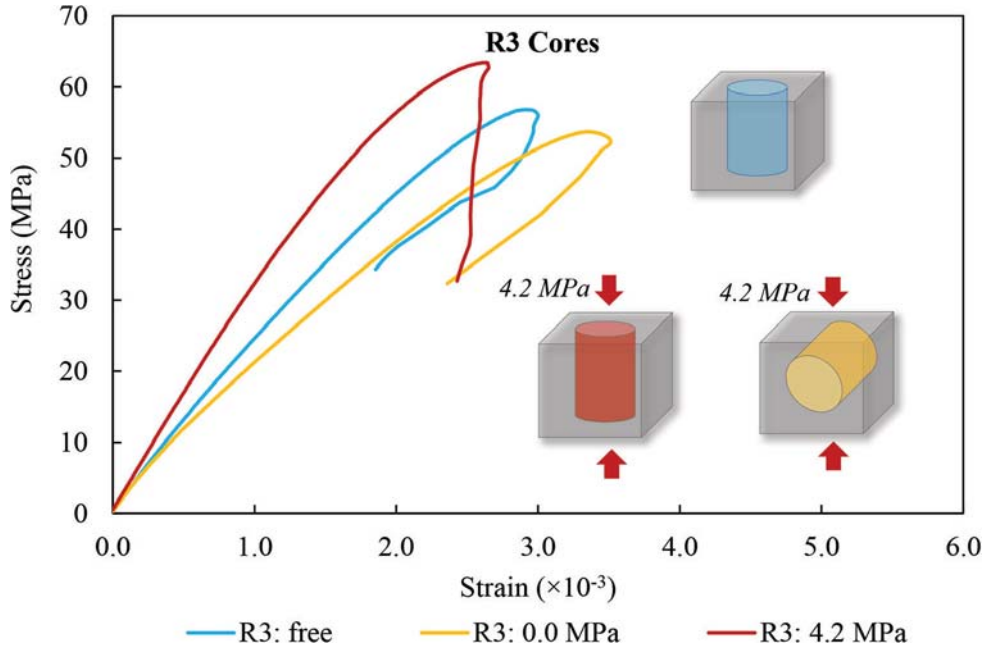

Fig. 10—Compression response R3 post-conditioning 3 in. Φ cores. (Note: 1 MPa = 145 psi.)

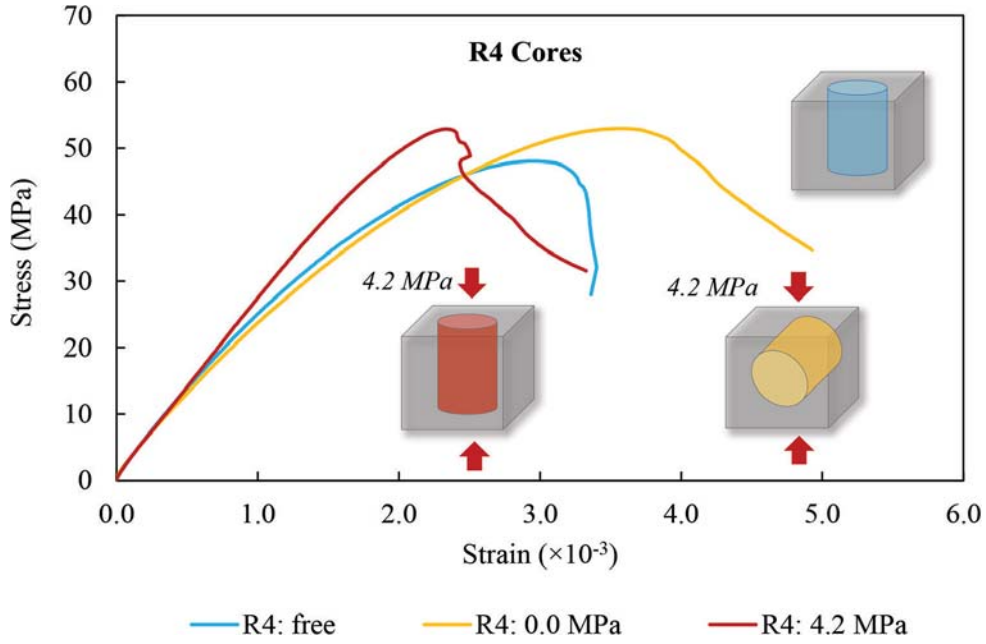

Fig. 11—Compression response R4 post-conditioning 3 in. Φ cores. (Note: 1 MPa = 145 psi.)

compressive stresses increased the splitting tensile strength along all directions compared to the unrestrained specimens. The splitting tensile strength of the Jobe-Newman cores, however, was not significantly influenced by the long-term stress condition.

Poisson's ratio—The Poisson's ratio was measured on cores during the post-conditioning compression tests. It was found to have a higher value for the specimens cored in the 4.2 MPa stress direction from all three Spratt casts, while it remained relatively unchanged for the remaining cores, compared to the values measured on cores extracted from the unrestrained specimens. For the Jobe-Newman cores extracted from the restrained cubes, the Poisson's ratio increased along all three directions compared to the cores extracted from the unrestrained cubes. For additional information, the reader is referred to Ferche.[33]

CONCLUSIONS

The primary purpose of the material-level test program was to investigate the evolution and the directionality of the mechanical properties of alkali-silica reaction (ASR)-affected concrete subjected to uniaxial and biaxial long-term compressive stresses. The results described herein contribute to expanding the limited database of tests on ASR-affected concrete elements previously reported in the literature. For the range of conditions examined, the following conclusions could be drawn:

1. ASR-induced deterioration affects differently the compressive strength, modulus of elasticity, and the tensile

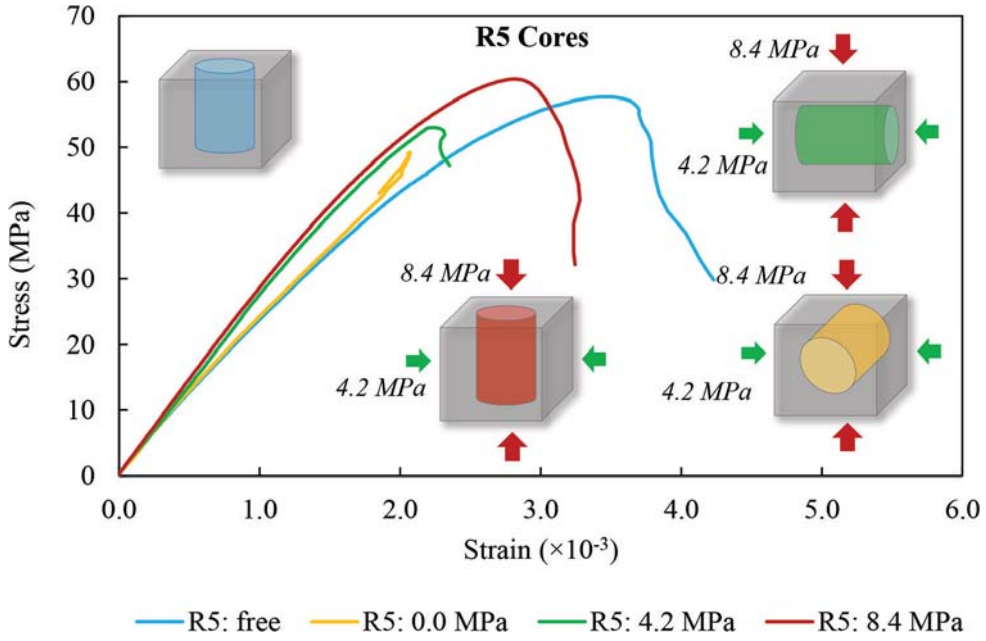

Fig. 12—Compression response R5 post-conditioning 3 in. Φ cores. (Note: 1 MPa = 145 psi.)

strength of concrete cured in stress-free conditions. For unrestrained ASR-induced strains in the 0.64×10^{-3} to 2.35×10^{-3} interval, there is a threshold which, if exceeded, triggers a mild to moderate degradation of the concrete compressive strength. The modulus of elasticity and tensile strength, on the other hand, are severely impacted for expansion levels as low as 0.64×10^{-3}.

2. The modulus of elasticity of reactive concrete is reduced by approximately 30% along an unrestrained direction for the range of ASR-induced expansion levels obtained in the current study; for broader ranges of expansion, the degree of degradation is dependent on the magnitude of the expansion. This reduction was measured for both unrestrained specimens and uniaxially or biaxially stressed ones.

3. The mechanical properties measured along an unrestrained direction of a concrete element subjected to sustained long-term uniaxial or biaxial compression are influenced by the coexisting orthogonal stresses. Tests performed on cores extracted from the first principal direction (that is, the unrestrained direction) of the restrained cubes exhibited a different behavior compared to cores extracted from unrestrained cubes made from the same mixture. However, the results showed large variability.

4. Long-term compressive stresses of 2.6 MPa and higher can essentially counteract the ASR-induced deterioration with respect to the concrete compressive strength along the restrained direction. The results obtained in this study suggest that, at such stress levels, the compressive strength of concrete remains virtually unaffected even with highly reactive mixtures.

5. The modulus of elasticity measured along the restrained directions is considerably more affected by ASR than the compressive strength. Compared to the compressive strength, a larger difference was observed between the values of the modulus of elasticity measured along the restrained and unrestrained directions. In other words, the anisotropy of the modulus of elasticity appears to be more pronounced compared to that of the compressive strength.

6. For unrestrained concrete specimens, the splitting tensile strength is affected to the same degree as the modulus of elasticity. The splitting tensile tests on cores extracted from the restrained cubes showed a larger variability compared to the unrestrained specimens. However, the trend observed indicated that the splitting tensile strength is less affected along the directions with long-term sustained compressive stresses compared to unrestrained directions.

7. The Poisson's ratio was measured during the post-conditioning compression tests. The Poisson's ratio had a higher value for the specimens cored in the 4.2 MPa stress direction from all three Spratt casts, while it remained relatively unchanged for the rest of the cores, compared to the values measured on cores extracted from the unrestrained specimens. For the Jobe-Newman cores extracted from the restrained cubes, the Poisson's ratio increased along all three directions compared to the cores extracted from the unrestrained cubes.

8. CSA A23.3 and ACI 318 Code equations for evaluating the modulus of elasticity as a function of the compressive strength are unconservative for ASR-affected concrete. This is due to the fact that ASR-induced deterioration mechanisms impact concrete strength and stiffness differently.

AUTHOR BIOS

Anca C. Ferche *is an Assistant Professor in the Department of Civil, Architectural and Environmental Engineering at The University of Texas at Austin, Austin, TX. She received her PhD from the University of Toronto, Toronto, ON, Canada, in 2020. Her research interests include performance assessment and analysis of reinforced concrete structures, concrete deterioration mechanisms, and rehabilitation of structures.*

Frank J. Vecchio, *FACI, is a Professor in the Department of Civil and Mineral Engineering at the University of Toronto. He is a member of Joint ACI-ASCE Committees 441, Reinforced Concrete Columns, and 447, Finite Element Analysis of Reinforced Concrete Structures. He is a recipient of the ACI Structural Research (1998), Structural Engineering (1999), Wason Medal for Most Meritorious Paper (2011), Joe W. Kelly (2016), and*

Arthur J. Boase (2020) awards. His research interests include advanced constitutive modeling and analysis of reinforced concrete and assessment and rehabilitation of structures.

ACKNOWLEDGMENTS

The authors would like to acknowledge NSERC for funding support provided to this project. The authors would also like to acknowledge the Ontario Ministry of Transportation and The University of Texas at Austin for providing the reactive aggregate.

REFERENCES

1. Stanton, T. E., "California Experience with the Expansion of Concrete through Reaction between Cement and Aggregate," *ACI Journal Proceedings*, V. 38, No. 3, Jan. 1942, pp. 209-215.

2. Stanton, T. E., "Expansion of Concrete through Reaction between Cement and Aggregate," *Proceedings of the American Society of Civil Engineers*, V. 66, No. 10, 1940, pp. 1781-1811. (Reprinted with discussion and closure in *Transaction, ASCE*, V. 107, pp. 54-126).

3. State of California Department of Transportation (NEPA Lead Agency) and City of Los Angeles, (CEQA Lead Agency), "6th Street Viaduct Seismic Improvement Project (SCH#2007081005)," Los Angeles, CA, 2007, 5 pp.

4. den Uijl, J. A., and Kaptijn, N., "Shear Tests on Beams Cut from ASR-Affected Bridge Decks," *Large-Scale Structural Testing*, SP-211, M. A. Issa and Y. L. Mo, eds., American Concrete Institute, Farmington Hills, MI, Feb. 2003, pp. 115-134.

5. Hansen, S. G.; Barbosa, R. A.; Hoang, L. C.; and Hansen, K. K., "Shear Capacity of ASR Damaged Structures—In-Depth Analysis of Some in-situ Shear Tests on Bridge Slabs," *Proceedings of the 15th International Conference on Alkali-Aggregate Reaction in Concrete*, Sao Paulo, Brazil, 2016, pp. 1-10.

6. Sanchez, L. F. M.; Fournier, B.; Mitchell, D.; and Bastien, J., "Condition Assessment of an ASR-Affected Overpass after Nearly 50 Years in Service," *Construction and Building Materials*, V. 236, Mar. 2020, Article No. 117554. doi: 10.1016/j.conbuildmat.2019.117554

7. Gautam, B. P.; Panesar, D. K.; Sheikh, S. A.; and Vecchio, F. J., "Effect of Coarse Aggregate Grading on the ASR Expansion and Damage of Concrete," *Cement and Concrete Research*, V. 95, May 2017, pp. 75-83. doi: 10.1016/j.cemconres.2017.02.022

8. Smaoui, N.; Bérubé, M. A.; Fournier, B.; and Bissonnette, B., "Influence of Specimen Geometry, Orientation of Casting Plane, and Mode of Concrete Consolidation on Expansion due to ASR," *Cement, Concrete and Aggregates*, V. 26, No. 2, 2004, pp. 58-70. doi: 10.1520/CCA11927

9. Ahmed, T.; Burley, E.; Rigden, S.; and Abu-Tair, A. I., "The Effect of Alkali Reactivity on the Mechanical Properties of Concrete," *Construction and Building Materials*, V. 17, No. 2, 2003, pp. 123-144. doi: 10.1016/S0950-0618(02)00009-0

10. Multon, S.; Cyr, M.; Sellier, A.; Diederich, P.; and Petit, L., "Effects of Aggregate Size and Alkali Content on ASR Expansion," *Cement and Concrete Research*, V. 40, No. 4, 2010, pp. 508-516. doi: 10.1016/j.cemconres.2009.08.002

11. Gautam, B. P., and Panesar, D. K., "The Effect of Elevated Conditioning Temperature on the ASR Expansion, Cracking and Properties of Reactive Spratt Aggregate Concrete," *Construction and Building Materials*, V. 140, June 2017, pp. 310-320. doi: 10.1016/j.conbuildmat.2017.02.104

12. Larive, C.; Laplaud, A.; and Coussy, O., "The Role of Water in Alkali-Silica Reaction," *Proceedings of the 11th International Conference on Alkali-Aggregate Reaction*, Quebec, QC, Canada, 2000, pp. 61-69.

13. Collins, R. J., and Bareham, P. D., "Alkali-Silica Reaction: Suppression of Expansion Using Porous Aggregate," *Cement and Concrete Research*, V. 17, No. 1, 1987, pp. 89-96. doi: 10.1016/0008-8846(87)90063-9

14. Wald, D. M.; Allford, M. T.; Bayrak, O.; and Hrynyk, T. D., "Development and Multiaxial Distribution of Expansions in Reinforced Concrete Elements Affected by Alkali–Silica Reaction," *Structural Concrete*, V. 18, No. 6, 2017, pp. 914-928. doi: 10.1002/suco.201600220

15. Berra, M.; Faggiani, G.; Mangialardi, T.; and Paolini, A. E., "Influence of Stress Restraint on the Expansive Behaviour of Concrete Affected by Alkali-Silica Reaction," *Cement and Concrete Research*, V. 40, No. 9, 2010, pp. 1403-1409. doi: 10.1016/j.cemconres.2010.05.002

16. Multon, S., and Toutlemonde, F., "Effect of Applied Stresses on Alkali–Silica Reaction-Induced Expansions," *Cement and Concrete Research*, V. 36, No. 5, 2006, pp. 912-920. doi: 10.1016/j.cemconres.2005.11.012

17. Kagimoto, H.; Yasuda, Y.; and Kawamura, M., "ASR Expansion, Expansive Pressure and Cracking in Concrete Prisms under Various Degrees of Restraint," *Cement and Concrete Research*, V. 59, May 2014, pp. 1-15. doi: 10.1016/j.cemconres.2014.01.018

18. Giannini, E. R.; Bentivegna, A. F.; and Folliard, K. J., "Strain Gradients in Concrete Affected by Alkali-Silica Reaction: A Laboratory Simulation," *Advances in Civil Engineering Materials*, V. 3, No. 1, 2014, pp. 388-403. doi: 10.1520/ACEM20130114

19. Liaudat, J.; Carol, I.; López, C. M.; and Saouma, V. E., "ASR Expansions in Concrete under Triaxial Confinement," *Cement and Concrete Composites*, V. 86, June 2018, pp. 160-170. doi: 10.1016/j.cemconcomp.2017.10.010

20. Barbosa, R. A.; Hansen, S. G.; Hansen, K. K.; Hoang, L. C.; and Grelk, B., "Influence of Alkali-Silica Reaction and Crack Orientation on the Uniaxial Compressive Strength of Concrete Cores from Slab Bridges," *Construction and Building Materials*, V. 176, July 2018, pp. 440-451. doi: 10.1016/j.conbuildmat.2018.03.096

21. Gautam, B. P.; Panesar, D. K.; Sheikh, S. A.; and Vecchio, F. J., "Effect of Multiaxial Stresses on Alkali-Silica Reaction Damage of Concrete," *ACI Materials Journal*, V. 114, No. 4, July-Aug. 2017, pp. 595-604. doi: 10.14359/51689617

22. Giaccio, G.; Torrijos, M. C.; Tobes, J. M.; Batic, O. R.; and Zerbino, R., "Development of Alkali-Silica Reaction under Compressive Loading and Its Effects on Concrete Behavior," *ACI Materials Journal*, V. 106, No. 3, May-June 2009, pp. 223-230.

23. ASTM C1293-09, "Standard Test Method for Determination of Length Change of Concrete due to Alkali-Silica Reaction," ASTM International, West Conshohocken, PA, 2009, 7 pp.

24. Rogers, C., and MacDonald, C. A., "The Geology, Properties and Field Performance of Alkali-Aggregate Reactive Spratt, Sudbury and Pittsburg Aggregate Distributed by the Ontario Ministry of Transportation," *Proceedings of the Fourteenth International Conference on Alkali-Aggregate Reaction (ICAAR)*, Austin, TX, 2012, 10 pp.

25. Deschenes, D. J., "ASR/DEF—Damaged Bent Caps: Shear Tests and Field Implications," Master's thesis, The University of Texas at Austin, Austin, TX, 2009, 271 pp.

26. Gautam, B. P., and Panesar, D. K., "A New Method of Applying Long-Term Multiaxial Stresses in Concrete Specimens Undergoing ASR, and Their Triaxial Expansions," *Materials and Structures*, V. 49, No. 9, 2016, pp. 3495-3508. doi: 10.1617/s11527-015-0734-z

27. Locher, F. W., and Sprung, F., "Ursache und Wirkungsweise der Alkalireacktion," *Beton*, V. 23, No. 7&8, 1973, 23 pp. (in German)

28. CSA A23.1-14/A23.2-14, "Concrete Materials and Methods of Concrete Construction/Test Methods and Standard Practices for Concrete," CSA Group, Toronto, ON, Canada, 2014, 690 pp.

29. Habibi, F.; Sheikh, S. A.; Vecchio, F. J.; and Panesar, D., "Effects of Alkali-Silica Reaction on Concrete Squat Shear Walls," *ACI Structural Journal*, V. 115, No. 5, Sept. 2018, pp. 1329-1339. doi: 10.14359/51702238

30. ASTM C39/C39M-18, "Standard Test Method for Compressive Strength of Cylindrical Concrete Specimens," ASTM International, West Conshohocken, PA, 2018, 8 pp.

31. ASTM C469/C469M-14, "Standard Test Method for Static Modulus of Elasticity and Poisson's Ratio of Concrete in Compression," ASTM International, West Conshohocken, PA, 2014, 5 pp.

32. ASTM C496/C496M-17, "Standard Test Method for Splitting Tensile Strength of Cylindrical Concrete Specimens," ASTM International, West Conshohocken, PA, 2017, 5 pp.

33. Ferche, A.-C., "Behaviour and Modelling of ASR-Affected Shear-Critical Reinforced Concrete Structures," PhD dissertation, Department of Civil and Mineral Engineering, University of Toronto, Toronto, ON, Canada, 2020, 392 pp.

34. Kozul, R., and Darwin, D., "Effects of Aggregate Type, Size, and Content on Concrete Strength and Fracture Energy," *SM Report No. 43*, University of Kansas Center for Research, Lawrence, KS, June 1997, 98 pp.

35. Sanchez, L. F. M.; Fournier, B.; Jolin, M.; Mitchell, D.; and Bastien, J., "Overall Assessment of Alkali-Aggregate Reaction (AAR) in Concretes Presenting Different Strengths and Incorporating a Wide Range of Reactive Aggregate Types and Natures," *Cement and Concrete Research*, V. 93, Mar. 2017, pp. 17-31. doi: 10.1016/j.cemconres.2016.12.001

36. CSA A23.3-14, "Design of Concrete Structures," CSA Group, Toronto, ON, Canada, 2014, 456 pp.

37. ACI Committee 318, "Building Code Requirements for Structural Concrete (ACI 318-19) and Commentary (ACI 318R-19)," American Concrete Institute, Farmington Hills, MI, 2019, 624 pp.